

Tomographic test of Bell's inequality

G M D'Ariano[†], L Maccone[†], M F Sacchi[†] and A Garuccio[‡]

[†] Theoretical Quantum Optics Group, Università degli Studi di Pavia, INFN—Unità di Pavia, via A Bassi 6, I-27100 Pavia, Italy

[‡] Dipartimento Interateneo di Fisica, INFN, Sezione D, I-70126 Bari, Italy

Received 8 April 1999, in final form 30 July 1999

Abstract. We present a homodyne detection scheme to verify Bell's inequality on correlated optical beams at the output of a nondegenerate parametric amplifier. Our approach is based on tomographic measurement of the joint detection probabilities, which allows high quantum efficiency at detectors. A self-homodyne scheme is suggested to simplify the experimental set-up.

Keywords: Nonlocality, Bell's inequality, quantum tomography

1. Introduction

In 1935 Einstein *et al* [1] proved the incompatibility of three hypotheses: (1) quantum mechanics is correct; (2) quantum mechanics is complete; (3) the following criterion of local reality holds: 'If, without in any way disturbing a system, we can predict with certainty [...] the value of a physical quantity, then there exists an element of physical reality corresponding to this quantity.' The paper opened a long and as yet unsettled debate about which one of the three hypotheses should be discarded. While Einstein suggested abandoning the completeness of quantum mechanics, Bohr [2] rejected the criterion of reality. The most important step forward in this debate was Bell's theorem of 1964 [3], which proved that there is an intrinsic incompatibility between assumptions (1) and (3), namely the correctness of quantum mechanics and Einstein's 'criterion of reality'. In Bell's approach, a source produces a pair of correlated particles, which travel along opposite directions and impinge into two detectors. The two detectors measure two dichotomic observables $A(\alpha)$ and $B(\beta)$ respectively, α and β denoting experimental parameters which can be varied over different trials, typically the polarization/spin angle of detection at each apparatus. Assuming that each measurement outcome is determined by the experimental parameters α and β and by an 'element of reality' or 'hidden variable' λ , Bell proved an inequality which holds for any theory that satisfies Einstein's 'criterion of reality', while it is violated by quantum mechanics. Such a fundamental inequality, which allows an experimental discrimination between local hidden-variable theories and quantum mechanics, has been the focus of interest in a number of experimental works [4].

Unfortunately, Bell's proof is based on two conditions which are difficult to achieve experimentally. The first is the feasibility of an experimental configuration yielding perfect correlation; the second is the possibility of approaching an ideal measurement, which itself does not add randomness to the outcome. Since 1969, attention has focused on improving the correlation of the source on the one hand and, on the other,

on deriving more general inequalities that take into account detection quantum efficiency or circumvent the problem—however, at the cost of introducing supplementary hypotheses (see [5]), such as the well known 'fair sampling' assumption. It was clear to the authors of [5] that these assumptions were questionable, and, as a matter of fact, it was proved [6] that in all performed experimental checks the results can be reproduced in the context of Einstein's assumptions if the quantum efficiency of detectors is less than 82.3%. However, no experiment has yet succeeded in realizing such a high value of quantum efficiency.

In a typical experiment the source emits a pair of correlated photons and two detectors separately check the presence of the two photons after polarizing filters at angles α and β , respectively. Alternatively, one can use four photodetectors with polarizing beam splitters in front, with the advantage of checking through coincidence counts that photons come in pairs. Let us denote by $p_{\alpha,\beta}$ the joint probability of finding one photon at each detector with polarization angle α and β , respectively. In terms of the correlation function

$$C(\alpha, \beta) = p_{\alpha,\beta} + p_{\bar{\alpha},\bar{\beta}} - p_{\bar{\alpha},\beta} - p_{\alpha,\bar{\beta}}, \quad (1)$$

Bell's inequality [3] is expressed as

$$B(\alpha, \beta, \alpha', \beta') \doteq |C(\alpha, \beta) - C(\alpha, \beta')| + |C(\alpha', \beta') + C(\alpha', \beta)| \leq 2, \quad (2)$$

$\bar{\alpha}$ and $\bar{\beta}$ being the polarization angles orthogonal to α and β , respectively. In this paper we propose a new kind of test for Bell's inequality based on homodyne tomography [7,8] (for a review, see [9]). In our set-up the photodetectors are replaced by homodyne detectors, which along with the tomographic technique can be regarded as a black box for measuring the joint probabilities $p_{\alpha,\beta}$. The main advantage of the tomographic test is that it allows the use of linear photodiodes with quantum efficiency η higher than 90% [10]. On the other hand, the method works effectively even with η as low as 70%, without the need of a 'fair sampling' assumption,

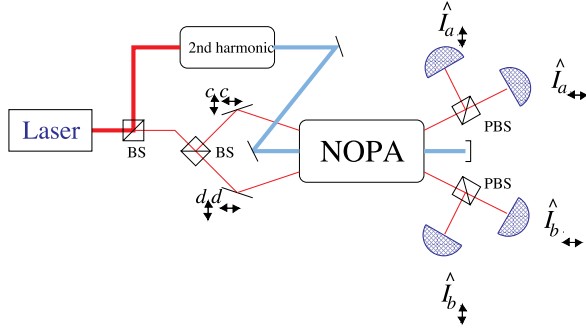


Figure 1. Experimental set-up for the tomographic test of Bell's inequality. PBS and BS denote 'polarizing beam splitter' and 'conventional beam splitter', respectively. Input radiation modes $a_{\dagger}, b_{\leftrightarrow}, a_{\leftrightarrow}, b_{\dagger}$ are in the vacuum state, while modes $c_{\dagger}, c_{\leftrightarrow}, d_{\dagger}, d_{\leftrightarrow}$ (at laser frequency ω_0) are in a coherent state. At the output of the nondegenerate parametric amplifier (NOPA) the four photocurrents \hat{I} at radiofrequency Ω are measured, yielding the value of quadratures of the field modes $a_{\dagger}, b_{\leftrightarrow}, a_{\leftrightarrow}$ and b_{\dagger} . The outcome quadratures are then used to reconstruct the probabilities of interest through quantum tomography.

since all data are collected in a single experimental run. With respect to the customary homodyne technique, which in the present case would need many beam splitters and local oscillators (LO) that are coherent each other, the set-up is greatly simplified by using the recent self-homodyne technique [11]. Another advantage of self-homodyning is the more efficient signal-LO mode-matching, with improved overall quantum efficiency.

2. The experimental set-up

The apparatus for generating the correlated beams is a $\chi^{(2)}$ nonlinear crystal, cut for type-II phase-matching, acting as a nondegenerate optical parametric amplifier (NOPA). The NOPA is injected with excited coherent states (see figure 1) in modes $c_{\leftrightarrow}, c_{\dagger}, d_{\leftrightarrow}, d_{\dagger}$ all with equal intensities and at the same frequency ω_0 ; c and d denote mode operators for the two different wavevector directions; and \dagger and \leftrightarrow represent vertical and horizontal polarization, respectively. The NOPA is pumped at the second harmonic $2\omega_0$. At the output of the amplifier four photodetectors separately measure the intensities $\hat{I}_{a_{\dagger}}, \hat{I}_{b_{\leftrightarrow}}, \hat{I}_{a_{\leftrightarrow}}, \hat{I}_{b_{\dagger}}$ of the mutual orthogonal polarization components of the fields propagating at different wavevectors. A narrow band of the photocurrent is selected, centred around frequency $\Omega \ll \omega_0$ (typically ω_0 is optical/infrared, whereas Ω is a radio frequency). In the process of direct detection, the central modes $c_{\dagger, \leftrightarrow}$ and $d_{\dagger, \leftrightarrow}$ beat with $\omega_0 \pm \Omega$ sidebands, thus playing the role of the LO of homodyne detectors. The four photocurrents $\hat{I}_{a_{\dagger}}, \hat{I}_{b_{\leftrightarrow}}, \hat{I}_{a_{\leftrightarrow}}, \hat{I}_{b_{\dagger}}$ yield the value of the quadratures of the four modes [11]

$$s_{\pi} = \frac{1}{\sqrt{2}}(a_{\pi}(+) + a_{\pi}(-)) \quad (3)$$

$$s = \{a, b\}, \quad \pi = \{\leftrightarrow, \dagger\},$$

where $a_{\pi}(\pm)$ and $b_{\pi}(\pm)$ denote the sideband modes at frequency $\omega_0 \pm \Omega$, which are in the vacuum state at the input of the NOPA. The quadrature is defined by the operator

$\hat{x}_{\phi} \doteq \frac{1}{2}(ae^{-i\phi} + a^{\dagger}e^{i\phi})$, where ϕ is the relative phase between the signal and the LO. The value of the quadratures is used as input data for the tomographic measurement of the correlation function $C(\alpha, \beta)$. The direction of polarizers (α, β) in the experimental set-up does not need to be varied over different trials, because, as we will show in the following, such direction can be changed tomographically.

We will now enter into details on the state at the output of the NOPA and on the tomographic detection. In terms of the field modes in equation (3) the spontaneous down-conversion at the NOPA is described by the unitary evolution operator

$$\hat{U}(\xi) = \exp[\xi(a_{\dagger}^{\dagger}b_{\leftrightarrow}^{\dagger} + e^{i\varphi}a_{\leftrightarrow}^{\dagger}b_{\dagger}^{\dagger}) - \text{h.c.}], \quad (4)$$

where $\xi = \chi^{(2)}\gamma L/c$ is a rescaled interaction time written in terms of the nonlinear susceptibility $\chi^{(2)}$ of the medium, the crystal length L , the pump amplitude γ and the speed c of light in the medium, whereas φ represents a tunable phase that can be varied by rotating the crystal around the optical axis [12]. The state at the output of the NOPA is expressed as

$$|\psi\rangle = (1 - |\Lambda|^2) \sum_{n=0}^{\infty} \sum_{m=0}^{\infty} \Lambda^{n+m} e^{i\varphi m} |n, n, m, m\rangle$$

$$\equiv |\psi_{1,2}\rangle \otimes |\psi_{3,4}\rangle, \quad (5)$$

where $\Lambda = \xi/|\xi| \tanh|\xi|$ and $|i, l, m, n\rangle$ represents the common eigenvector of the number operators of modes $a_{\dagger}, b_{\leftrightarrow}, a_{\leftrightarrow}, b_{\dagger}$, with eigenvalues i, l, m and n , respectively. The average photon number *per* mode is given by $N = |\Lambda|^2/(1 - |\Lambda|^2)$. The four-mode state vector in equation (5) factorizes into a couple of twin beams $|\psi_{1,2}\rangle$ and $|\psi_{3,4}\rangle$, each one entangling a couple of spatially divergent modes ($a_{\dagger}, b_{\leftrightarrow}$ and $a_{\leftrightarrow}, b_{\dagger}$, respectively).

Notice that conventional experiments, concerning a two-photon polarization-entangled state generated by spontaneous down-conversion, consider a four-mode entangled state which corresponds to keeping only the first-order terms of the sums in equation (5), and to ignoring the vacuum component, as only intensity correlations are usually measured. Here, in contrast, we measure the joint probabilities on the state (5) to test Bell's inequality through homodyne tomography, which yields the value of $B(\alpha, \beta, \alpha', \beta')$ in equation (2).

3. Tomographic test of Bell's inequality

The tomographic technique is a kind of universal detector, which can measure any observable \hat{O} of the field, by averaging a suitable 'pattern' function $\mathcal{R}[\hat{O}](x, \phi)$ over homodyne data x at random phase ϕ . The 'pattern' function is obtained through the trace rule [13]:

$$\mathcal{R}[\hat{O}](x, \phi) = \text{Tr}[\hat{O}K_{\eta}(x - \hat{x}_{\phi})], \quad (6)$$

where $K_{\eta}(x)$ is a distribution given in [14]. For factorized many-mode operators $\hat{O} = \hat{O}_1 \otimes \hat{O}_2 \otimes \dots \otimes \hat{O}_n$ the pattern function is just the product of those corresponding to each single-mode operator $\hat{O}_1, \dots, \hat{O}_n$ labelled by variables $(x_1, \phi_1), \dots, (x_n, \phi_n)$. By linearity the pattern function is extended to generic many-mode operators.

Now we consider which observables are involved in testing Bell's inequality (2). Let us denote by $q_{\alpha,\beta}(i, l, m, n)$ the probability of having i, l, m, n photons in modes $a_{\uparrow}, b_{\leftrightarrow}, a_{\leftrightarrow}, b_{\uparrow}$ for the 'rotated' state

$$|\psi\rangle_{\alpha,\beta} \equiv \hat{U}_{1,3}(\alpha)\hat{U}_{2,4}(\beta)|\psi\rangle, \quad (7)$$

$\hat{U}_{1,3}(\alpha)$ and $\hat{U}_{2,4}(\beta)$ being the unitary operators

$$\hat{U}_{1,3}(\alpha) = \exp[\alpha(a_{\uparrow}^{\dagger}a_{\leftrightarrow} - a_{\uparrow}a_{\leftrightarrow}^{\dagger})], \quad (8)$$

$$\hat{U}_{2,4}(\beta) = \exp[\beta(b_{\uparrow}^{\dagger}b_{\leftrightarrow} - b_{\uparrow}b_{\leftrightarrow}^{\dagger})]. \quad (9)$$

The probabilities in equation (1) can be written as $p_{\alpha,\beta} = p_{\alpha,\beta}(1, 1)$, $p_{\bar{\alpha},\bar{\beta}} = p_{\alpha,\beta}(0, 0)$, $p_{\bar{\alpha},\beta} = p_{\alpha,\beta}(0, 1)$, and $p_{\alpha,\bar{\beta}} = p_{\alpha,\beta}(1, 0)$, with

$$p_{\alpha,\beta}(n, m) = \frac{q_{\alpha,\beta}(n, 1-m, 1-n, m)}{P(1, 1)}, \quad (10)$$

and $\{n, m = 0, 1\}$. The denominator $P(1, 1)$ in equation (10) represents the absolute probability of having at the output of the NOPA one photon in modes $a_{\uparrow}, a_{\leftrightarrow}$ and one photon in modes $b_{\uparrow}, b_{\leftrightarrow}$, independently on the polarization, namely

$$P(1, 1) = \sum_{n=0,1} \sum_{m=0,1} q_{\alpha,\beta}(n, 1-m, 1-n, m). \quad (11)$$

Notice that our procedure does not need a fair sampling assumption since we measure in only one run both the numerator and the denominator of equation (10): namely we do not have to collect auxiliary data to normalize probabilities. On the other hand, since we can exploit quantum efficiencies as high as $\eta = 90\%$ or more, and the tomographic pattern functions already take into account η , we do not need a supplementary hypothesis for it.

The observables that correspond to probabilities $q_{\alpha,\beta}(i, l, m, n)$ in equations (10) and (11) are

$$\begin{aligned} &|i, l, m, n\rangle_{\alpha,\beta} \equiv |i, l, m, n\rangle \\ &= \hat{U}_{1,3}^{\dagger}(\alpha)\hat{U}_{2,4}^{\dagger}(\beta)|i, l, m, n\rangle \langle i, l, m, n|\hat{U}_{2,4}(\beta)\hat{U}_{1,3}(\alpha). \end{aligned} \quad (12)$$

After a straightforward calculation using equations (10)–(12), one obtains that $P(1, 1)$ is measured through the following average \mathcal{AV} of homodyne data:

$$P(1, 1) = \mathcal{AV}\{(K_1^1 K_0^3 + K_0^1 K_1^3)(K_1^2 K_0^4 + K_0^2 K_1^4)\}, \quad (13)$$

where K_n^j denotes the diagonal ($n = 0, 1$) tomographic kernel function for mode j , namely

$$K_n^j \equiv \langle n|K_{\eta}(x - \hat{x}_{\phi_j})|n\rangle. \quad (14)$$

The probabilities in the numerator of equation (10) are given by the average of a lengthy expression, which depends on both the diagonal terms (14) and the following off-diagonal terms:

$$\begin{aligned} K_+^j &\equiv \langle 0|K_{\eta}(x - \hat{x}_{\phi_j})|1\rangle, \\ K_-^j &\equiv \langle 1|K_{\eta}(x - \hat{x}_{\phi_j})|0\rangle = (K_+^j)^*. \end{aligned} \quad (15)$$

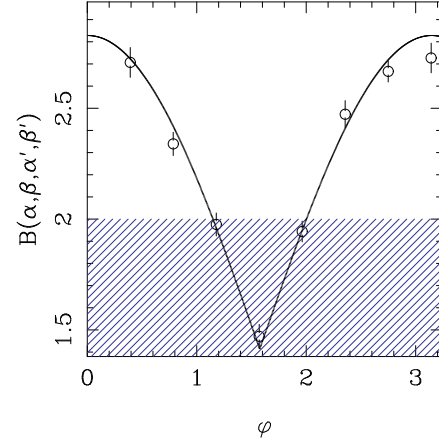


Figure 2. Plot of $B(\alpha, \beta, \alpha', \beta')$ versus the phase ϕ in the state of equation (5) for a simulated experiment. The shaded area represents the classical region for B . The parameters of the simulation are: $\alpha = 0$; $\beta = \frac{3}{8}\pi$; $\alpha' = \frac{\pi}{4}$; $\beta' = \frac{\pi}{8}$; quantum efficiency $\eta = 85\%$; average photon number *per mode* $N = 0.5$. A total number of 10^6 homodyne data (divided into 20 statistical blocks) has been used.

Here we report the final expression for $C(\alpha, \beta)$ of equation (1):

$$\begin{aligned} C(\alpha, \beta) &= \frac{1}{P(1, 1)} \mathcal{AV}\{[\cos(2\alpha)(K_1^1 K_0^3 - K_0^1 K_1^3) \\ &+ \sin(2\alpha)(K_+^1 K_-^3 + K_-^1 K_+^3)] \\ &\times [\cos(2\beta)(K_0^2 K_1^4 - K_1^2 K_0^4) \\ &+ \sin(2\beta)(K_+^2 K_-^4 + K_-^2 K_+^4)]\}. \end{aligned} \quad (16)$$

Caution must be taken in the estimation of the statistical error, because $C(\alpha, \beta)$ —and thus $B(\alpha, \beta, \alpha', \beta')$ in equation (2)—are nonlinear averages (they are ratios of averages). The error is obtained from the variance calculated upon dividing the set of data into large statistical blocks. However, since the nonlinearity of B introduces a systematical error which is vanishingly small for increasingly large sets of data, the estimated mean value of B is obtained from the full set of data, instead of averaging the mean value of blocks.

4. Numerical results

We now present some numerical results obtained from Monte Carlo simulations of the proposed experiment. For the simulation we use the theoretical homodyne probability pertaining to the state $|\psi\rangle$ in equation (5) which, for each factor $|\psi_{i,j}\rangle$, is given by

$$p_{\eta}(x_i, x_j; \phi_i, \phi_j) = \frac{2 \exp\left[-\frac{(x_i+x_j)^2}{d_{z_{ij}}^2 + 4\Delta_{\eta}^2} - \frac{(x_i-x_j)^2}{d_{-z_{ij}}^2 + 4\Delta_{\eta}^2}\right]}{\pi \sqrt{(d_{z_{ij}}^2 + 4\Delta_{\eta}^2)(d_{-z_{ij}}^2 + 4\Delta_{\eta}^2)}}, \quad (17)$$

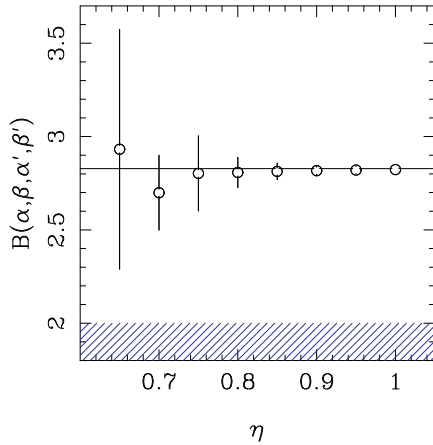


Figure 3. Plot of $B(\alpha, \beta, \alpha', \beta')$ versus the quantum efficiency of the detectors for a series of simulated experiments. The shaded area represents the classical region for B . The parameters of the simulations are: $\alpha = 0$; $\beta = \frac{3}{8}\pi$; $\alpha' = \frac{\pi}{4}$; $\beta' = \frac{\pi}{8}$; $\varphi = \pi$; $N = 0.5$. A total number of 6×10^7 homodyne data (in 20 statistical blocks) has been used for each simulation.

where x_i ($i = 1, 2, 3, 4$) is the outcome of the homodyne measurement for quadrature of the i th mode at phase ϕ_i , and

$$z_{ij} = e^{-i(\phi_i + \phi_j)} \Lambda, \quad d_{\pm z_{ij}}^2 = \frac{|1 \pm z_{ij}|^2}{1 - |z_{ij}|^2}, \quad (18)$$

$$\Delta_\eta^2 = \frac{1 - \eta}{4\eta}.$$

In figure 2 we present the simulation results for B in equation (2) versus the phase φ in the state of equation (5). The full line represents the value of B in equation (2) with the quantum theoretical value $C(\alpha, \beta)$ given by

$$C(\alpha, \beta) = \cos \varphi \sin 2\alpha \sin 2\beta - \cos 2\alpha \cos 2\beta. \quad (19)$$

Quantum efficiency $\eta = 85\%$ has been used; nonetheless, notice that for $\varphi = \pi$ (corresponding to a maximum violation with respect to the classical bound 2), the obtained value is over 10σ distant from the bound. By increasing the number of homodyne data, it is possible to also obtain good results for lower quantum efficiency. In fact, by increasing the number of data to 8×10^8 , a value of $B(0, \frac{3}{8}\pi, \frac{\pi}{4}, \frac{\pi}{8}) = 2.834 \pm 0.268$ has been obtained for $\Lambda = 0.5$, $\varphi = \pi$, and η as low as 65%. This result is to be compared with the quantum theoretical value of $2\sqrt{2}$. In figure 3 the results of the measurement of B , for different simulated experiments using the same number of data, are presented for different detector efficiencies η . Notice how the error bars decrease *versus* η .

For an order of magnitude of the data acquisition rate in a real experiment, one can consider that in a typical self-homodyne set-up with a NOPA pumped by a second harmonic of a Q-switched mode-locked Nd:YAG laser, the Q-switch and the mode-locker repetition rates are 10 kHz and 100 MHz, respectively. Typical time of the boxcar integration is 10 ns, so that one sample per pulse can be collected. In summary, 10^7 data samples can be obtained in 10^3 s. In such an experimental arrangement, for a Q-switch envelope of 200 ns, the shot noise can be reached by the peak amplitude of the

5 MHz low-pass-filtered photocurrent. For more detailed experimental parameters, the reader is referred to [15].

5. Conclusions

In conclusion, we have proposed a test of Bell's inequality, based on self-homodyne tomography. The rather simple experimental apparatus is mainly composed of a NOPA crystal and four photodiodes. The experimental data are collected through a self-homodyne scheme and processed by the tomographic technique. No supplementary hypotheses are introduced, a quantum efficiency η as high as 90% is currently available; in any case, η as low as 70% is tolerated for 10^6 – 10^7 experimental data. We have presented some numerical results based on Monte Carlo simulations that confirm the feasibility of the experiment, showing violations of Bell's inequality for over 10σ with detector quantum efficiency $\eta = 85\%$.

Acknowledgments

The authors thank the anonymous referee for his/her useful suggestions. The Quantum Optics Group of Pavia acknowledges the INFN for financial support (PRA-CAT97).

References

- [1] Einstein A, Podolsky B and Rosen N 1935 *Phys. Rev.* **47** 777
- [2] Bohr N 1935 *Phys. Rev.* **48** 696
- [3] Bell J S 1964 *Physics* **1** 195
- [4] Clauser J F 1976 *Phys. Rev. Lett.* **36** 1223
Aspect A, Dalibard J and Roger G 1981 *Phys. Rev. Lett.* **47** 460
Duncan A J, Perrie W, Beyer H J and Kleinpoppen H 1985 *Fundamental Processes in Atomic Collision Physics* (New York: Plenum) p 555
Ou Z Y and Mandel L 1988 *Phys. Rev. Lett.* **61** 50
Alley C O and Shih Y H 1988 *Phys. Rev. Lett.* **61** 2921
Franson J D 1989 *Phys. Rev. Lett.* **62** 2200
Mattle K, Weinfurter H, Kwiat P G and Zeilinger A 1996 *Phys. Rev. Lett.* **76** 4656
- [5] Clauser J F, Horne M A, Shimony A and Holt R A 1969 *Phys. Rev. Lett.* **23** 880
Clauser J F and Horne M A 1974 *Phys. Rev. D* **10** 256
Garuccio A and Rapisarda V A 1981 *Nuovo Cimento A* **65** 269
- [6] De Caro L and Garuccio A 1996 *Phys. Rev. A* **54** 174
- [7] Smithey D T, Beck M, Raymer M G and Faridani A 1993 *Phys. Rev. Lett.* **70** 1244
- [8] Breitenbach G, Schiller S and Mlynek J 1997 *Nature* **387** 471
- [9] D'Ariano G M 1997 Measuring quantum states *Quantum Optics and the Spectroscopy of Solids* ed T Hakioglu and A S Shumovsky (Dordrecht: Kluwer) p 175
- [10] Kim C and Kumar P 1994 *Phys. Rev. Lett.* **73** 1605
- [11] D'Ariano G M, Vasilyev M and Kumar P 1998 *Phys. Rev. A* **58** 636
- [12] Boschi D, De Martini F and Di Giuseppe G 1996 *Quantum Interferometry* ed F De Martini *et al* (Wenheim: VCH) p 135
- [13] D'Ariano G M 1997 *Quantum Communication, Computing and Measurement* ed O Hirota *et al* (New York: Plenum) p 253
- [14] D'Ariano G M, Leonhardt U and Paul H 1995 *Phys. Rev. A* **52** R1801
- [15] Vasilyev M, Choi S-K, Kumar P and D'Ariano G M 1998 *Opt. Lett.* **23** 1393